JOURNAL OF AIRCRAFT
Vol. 46, No. 1, January–February 2009

Modified Inertially Coupled Equations of Motion for Flexible Aircraft with Coupled Vibrations

Haroon A. Baluch* and Michel van Tooren†
Delft University of Technology, 2629 HS Delft, The Netherlands

DOI: 10.2514/1.36150

Use of the elastic axis to decouple the bending and torsion in vibration analysis does not work for fiber composite structures. Anisotropic material properties often result in an elastic axis that is either discontinuous or far outside the real aircraft. Existing mathematical models of flexible aircraft dynamics do not address this issue. In this paper, state-of-the-art inertially coupled equations of motion of a flexible aircraft are modified. For each of the equivalent beam models of the fuselage, wings, and tail structure a particular fixed axis is used as a reference of vibrations instead of using an elastic axis. Because no decoupling can be used, the beam deflections become a function of both bending and twist. The resulting displacements are expanded to the expressions of beam generalized velocities. This development also modifies the expressions of kinetic and strain energies and subsequent global mass and stiffness matrices, state-space coefficient matrices, and, finally, the structural loads equations. The effects of coupled vibrations on the aircraft dynamic response are simulated by placing the elastic axis of each wing and horizontal tail at three different positions with respect to a particular fixed reference axis. Results indicate that bending-torsion coupled vibrations significantly affect the aircraft response and thereby the structural loads.

Nomenclature

B_x	=	coefficient matrix with respect to aircraft motion
B_u	=	coefficient matrix with respect to control inputs
C	=	full-order damping matrix
C_i	=	component rotation matrix with respect to O_f
D	=	matrix of eigenvectors
d	=	eigenvector
$e_{1,2}$	=	null vectors of sizes 6×1 and $(6 + m) \times 1$
EI	=	bending stiffness of a section
F_d	=	dynamic shear force on a node
F_f	=	resultant force vector at O_f
G	=	closed-loop gain matrix
GJ	=	torsional stiffness of a section
I_i	=	local inertia matrix at a node of component i
J	=	cost function
K	=	full-order stiffness matrix
k	=	stiffness due to the material anisotropy
K_ξ	=	reduced-order stiffness matrix
L_f	=	generalized loads at O_f
L_η	=	reduced-order generalized structural loads
M	=	full-order global mass matrix
m	=	number of shape functions in reduced order
M_d	=	dynamic torsion moment on a node
M_f	=	resultant moment vector at O_f
M_ξ	=	reduced-order mass matrix
O_i	=	component origin
Q, R	=	weighting matrices in performance index
q, s	=	full-order generalized coordinates, velocities
Q_ψ	=	generalized force vector in torsion
r	=	distance of a node with respect to a component origin
R_f	=	translation vector $[R_{fx}, R_{fy}, R_{fz}]$ with respect to inertial axes
T	=	kinetic energy
t	=	time
u	=	control vector [elevator, aileron, rudder, thrust]
U_i	=	potential energy
y_i	=	distance between reference and elastic axes
α	=	rotation angles due to aft fuselage bending
ξ	=	reduced-order generalized coordinates
η	=	reduced-order generalized velocities
θ_f	=	rotation vector [roll, pitch, yaw] $[\theta_{f\Phi}, \theta_{f\theta}, \theta_{f\Psi}]$
λ	=	eigenvalue
ϕ	=	matrix of component shape functions

Subscripts

e	=	empennage
f	=	fuselage
g	=	gust
i	=	referring to a particular component
jk	=	rows and column in a matrix
n	=	number of sections over the length of a beam
u	=	degree of freedom in bending
w	=	wing
ψ	=	degree of freedom in torsion

Superscripts

A	=	aft
F	=	fore
L	=	left
R	=	right
V	=	vertical
T	=	transpose
(0)	=	zero order
(1)	=	first order
$\tilde{}$	=	skew symmetric matrix of a vector

Received 11 December 2007; accepted for publication 14 October 2008.

*Ph.D. Student, Faculty of Aerospace Engineering, Kluyverweg 1; h.a.baluch@tudelft.nl. Student Member AIAA.

†Professor, Faculty of Aerospace Engineering, Kluyverweg 1; m.j.l.vanTooren@tudelft.nl. Member AIAA.

I. Introduction

THE mathematical modeling of maneuvering flexible aircraft is in constant evolution. The main reason behind the evolution can be the availability of fast computers, which allow one to simulate from a simple model to a quite complex model, addressing the trinity of flight dynamics, controls, and aeroelasticity in one simulation. Previously their capabilities were limited to simple models, which forced the engineers to make a lot of approximations during the mathematical modeling. The emergence of high-altitude and

long-endurance unmanned aerial vehicles with high aspect ratio flexible wings, subject to large wing deflections in flight, have opened a new scope in the modeling and simulation of highly flexible aircraft by adding the structural nonlinearities in the mathematical model [1]. We intend to keep the scope of our present work to a model, which allows us to consider only the small perturbations around the steady-state condition and developing a linear aircraft model, useful for simulation from a small business jet [2] to a large transport airplane [3]. Although a linear model is only valid close to the reference condition, at the same time it fulfills the requirements in simulating the different flight load conditions prescribed in aviation regulations for light and large aeroplanes like FAR/CS part 23 and part 25, respectively.

One of the simplifications is the use of such reference axes as aircraft body axes, usually called "mean axes," which are not fixed with a material point on the fuselage [4,5]. There are two consequences of using mean axes as body axes. First, omission of the linear and angular momenta due to elastic deformation in the total kinetic energy of the aircraft (i.e., the derivatives of the Lagrangian of the whole aircraft with respect to local structural velocities are zero in those equations that belong to the rigid-body motion of the aircraft), hence it inertially decouples the two sets of equations (i.e., flight and structural dynamics). The only coupling between these two sets of equations is achieved through the aerodynamic forces [3,5]. Second, the use of free–free orthogonal mode shapes that decouple the structural dynamics equations and constructs a diagonal[‡] mass matrix [3,5]. In short, a vibrating fuselage does not affect the wings or tail planes through inertial terms and vice versa.

Lately, by using the quasi-coordinate approach, Tuzcu and Meirovitch [2] show the replacement of mean axes by another kind of aircraft body axes, called "body fixed axes," which are fixed with a material point of the fuselage. The aircraft structural components like fuselage, wings, and empennage are represented in the form of equivalent beams with fixed–free mode shapes. The equations of motion are inertially coupled by taking into account the effects of linear and angular momenta due to elastic deformation in the total kinetic energy of the aircraft, hence giving a nondiagonal mass matrix. Most recently these inertially coupled equations of motion are extended to the simulation of dynamic loads during atmospheric turbulence [7]. In all the cases mentioned, the stiffness matrix is always diagonal (i.e., without the cross coupling terms of bending and torsion degrees of freedom [2,3,5,7]). The primary factor behind a diagonal stiffness matrix of a beam is the use of its elastic axis ($e.a$) as a reference to calculate the deformations. The cross coupling terms in a stiffness matrix may appear in cases where the reference axis to which deformations are calculated is not an elastic axis or due to anisotropic material properties. Anisotropy, in the case of fiber composite structures, appears when the principal axis of the laminate is not aligned with the reference axis of the structure.

In aeroelastic tailoring (e.g., to increase the divergence and flutter speeds) the optimized design often suggests different combinations of skin thickness and fiber orientations [8]. It shows that the flutter speed in the case of asymmetric laminates with respect to the midplane is increased as much as 20% compared with those from symmetric laminates, but the asymmetry introduces cross coupling terms in the stiffness matrix. Previously, research on the box beam of a helicopter blade shows that even the symmetric laminates of each flange and web contribute to the cross coupling terms with an appreciable influence on the stability of the blade [9]. Although the laminates of each side of the box beam are symmetric with respect to their respective midplanes, several fibers in a laminate of a particular flange or web are not aligned with the reference plane, resulting in a bending–torsion coupling. Later on, the deformations calculated analytically in [9] were correlated with experimental results with satisfactory conformity [10].

[‡]In this paper a diagonal or nondiagonal matrix means a "block" diagonal or nondiagonal matrix, respectively. A block diagonal matrix is defined as a square matrix in which the diagonal elements are square matrices of any size, and the off-diagonal elements are zero [6].

The elements of a stiffness matrix depend upon cross-sectional properties as well as the material properties (i.e., the stiffnesses along the bending and torsion directions). The moduli of metal alloys are well determined and published in the literature. In cases of fiber composite, it largely depends upon the stacking sequence of the fibers and requires some analytical formulas to construct the stiffness matrix. In addition to [9,10], an excellent paper by Smith and Chopra [11] also gives a detailed analytical model of constructing the stiffness matrix for a thin-walled fiber composite helicopter blade. Although this model takes care of calculating stiffness along a bending–extension degree of freedom (DOF), which is generally not incorporated in a fixed-wing aircraft, one can use the model by omitting the bending–extension coupling in the stiffness matrix. Moreover, Lottati [12] also gives an overview on how to construct the stiffness matrix for a composite wing with anisotropic material properties.

For a beam element with isotropic material properties, the shear center of a particular section plays a significant role in decoupling the bending and torsion deformations, where the coupling becomes a cross-sectional property [13]. Hodges [13] presents a method that describes how to find generalized shear centers of several sections along the beam length. The elastic axis intersects with these centers. It is most likely that while optimizing a composite wing structure, one will come up with a design that requires asymmetric fibers orientation with respect to the laminate midplane. In this situation a nondiagonal stiffness matrix due to anisotropic material properties is quite obvious. Furthermore, during the optimization process one can also get different positions of a shear center of a particular section of a component. It can be out of the structural boundaries near the tip of a wing, and the resultant elastic axis might not be exhibiting a straight line from root to tip. Even then if one insists on using the elastic axis as a reference, the cross coupling terms in the stiffness matrix gives a shear deformation due to bending moment. Otherwise, as suggested by Hodges [13], the locus of mass centroids as being a reference line can be an alternative to the elastic axis, but the straightness of this line is also not guaranteed due to structural discontinuities in fixed-wing aircrafts.

Keeping in mind the increasing use of fiber composite material in aircraft structures, a mathematical model is looked for that does not have the necessity of using the $e.a$ as references of vibrations in aircraft components. The use of the $e.a$ of a component is to be replaced by a "practical" reference axis $r.a$ and its location on each component of the aircraft is fixed at a certain position relative to the aircraft body axes. The use of $r.a$ was already shown in [12]. But the mathematical modeling was restricted only to a wing structure for flutter analysis. The aim of this paper is to address the dynamics of the whole aircraft, which, as stated, includes the trio of flight dynamics, controls, and aeroelasticity in one simulation. The preference is to modify the existing mathematical model, rather than "reinventing the wheel." In this paper we choose the mathematical model derived by Tuzcu and Meirovitch [2] as our base model for the modifications. Besides the introduction of coupling due to material properties in the stiffness matrix, the use of practical reference axes also incorporates the use of bending–torsion coupled beams in the structural model and modifies the equations of motion. The chosen mathematical model is based on a purely analytical approach. Introducing the bending–torsion coupling makes the equations more complex. It starts by redefining the deflection of a beam section in bending to incorporate the torsion effects. The result is expanded to the modified expressions of beam generalized velocities. The modified expressions of generalized velocities and deflections affect the whole mathematical model from top to bottom (i.e., from the equations of kinetic and strain energies to the global mass and stiffness matrices, respectively) and further down to state-space coefficient matrices and structural load equations.

The structure of this paper is as follows. Section II presents the mathematical modeling with all those steps that are taken during the modification process and are believed necessary to be included in this paper. A dynamic loads model is presented in Sec. III. Presenting a complete structural optimization problem, which also includes finding the cross-sectional and material properties, is out of the scope

of this paper, but the modified equations of motion do present a viable basis to do so. Moreover, due to the lack of available structural data of the composite aircraft, it is not possible to include the cross couplings in the stiffness matrix due to anisotropic materials properties. To anyway simulate the effects of coupling on the response and subsequent loads, three different positions of $e.a$ with respect to a particular fixed $r.a$ on wing and tailplane of a twin-jet metal aircraft are considered in a numerical example of Sec. IV, where the aircraft is subjected to a discrete gust. Finally, the conclusions are made in Sec. V.

II. Mathematical Modeling

The structure of a flexible aircraft can be discretized into a number of beams. Figure 1 shows a sample aircraft modeled with seven beams to represent fore and aft fuselage structures, one beam per half wing and half horizontal tail, and one beam for the vertical tail, where the aircraft body axis O_f lies on the juncture of aft and fore fuselages beams. These beams are further discretized into several sections with lumped mass elements m_i at their mass centers $(c.g)$. These mass elements are attached to each other with springs of average stiffness over the two neighboring sections. For each fuselage beam there are two bending DOF u along each y and z direction of the aircraft body axes O_f and one torsion ψ along the longitudinal axis of O_f [2]. For each wing and empennage beam there is one bending DOF normal to the plane of the lifting surface and one torsion DOF along the $r.a$ (i.e., longitudinal axis of their respective coordinate axes at O_i).

The aerodynamic model is essentially a two-dimensional model, presented in the form of several strips with lift, moment, and drag coefficients. The quasi-steady forces and moments on each strip are functions of these coefficients and the local angle of attack of the strip. The instantaneous local angle of attack of a strip is determined from the torsion angle ψ of that strip and the rigid-body angle, which includes the aircraft pitch angle at O_f and the incidence of the lifting surface at its attachment with the fuselage. It is known that the aeroelastic predictions are usually conservative when using the quasi-steady strip theory [14], but at the same time the use of aerodynamic coefficients suits the quasi-coordinate approach [2]. Otherwise the aerodynamic data from a high fidelity analysis (e.g., computational fluid dynamics or wind tunnel testing) can also be converted to aerodynamic coefficients and the same form of the equations of motion can be used [15].

The rigid-body motion of an aircraft can be expressed into a vector of three translational velocities V_f and a vector of three rotational velocities Ω_f around the body axes O_f of the aircraft. The total kinetic energy T due to rigid and elastic motions of the aircraft will be as follows [2]:

$$T = \frac{1}{2}\int \overline{V}_f^T \overline{V}_f dm_f + \frac{1}{2}\int \overline{V}_w^T \overline{V}_w dm_w + \frac{1}{2}\int \overline{V}_e^T \overline{V}_e dm_e = \frac{1}{2} V^T M V \tag{1}$$

where the discrete velocity vector is as follows:

$$V = [\,V_f^T \quad \Omega_f^T \quad s_{uf}^T \quad s_{uw}^T \quad s_{ue}^T \quad s_{\psi f}^T \quad s_{\psi w}^T \quad s_{\psi e}^T\,]^T \tag{2}$$

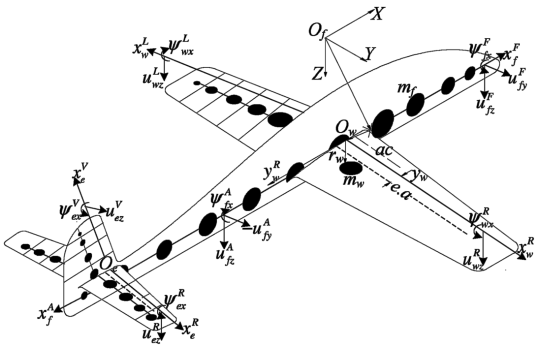

Fig. 1 Aircraft discretized model.

The local elastic motion of a component is expressed in the form of generalized structural velocities $s_{u,\psi}$. Before defining the expressions of each velocity subvectors in Eq. (2), first the structural deflections of a section of a component i, placed at a distance r_i from its origin O_i, are defined. Figure 2 shows a deformed section, where z_i, u_i, and ψ_i represent the total vertical deflection, pure bending, and torsion, respectively. While assuming no shear deformation along the cross section [14] and using the small angle approximation in conjunction with the Galerkin method, the deformations with respect to the $r.a$ of a component are expressed as a function of two shape functions $\phi_{u,\psi}$ per DOF of a fixed–free beam and the corresponding vector of generalized coordinates $q_{u,\psi}$:

$$z_i(r_i,t) = u_i + y_i \sin(\psi_i(r_i,t)) = \phi_{ui}(r_i)q_{ui}(t) + y_i\phi_{\psi i}(r_i)q_{\psi i}(t)$$
$$\psi_i(r_i,t) = \phi_{\psi i}(r_i)q_{\psi i}(t) \tag{3}$$

By taking the time derivative of the generalized coordinates, the corresponding structural velocities will be as follows:

$$\dot{z}_i(r_i,t) = \phi_{ui}(r_i)s_{ui}(t) + y_i\phi_{\psi i}(r_i)s_{\psi i}(t)$$
$$\dot{\psi}_i(r_i,t) = \phi_{\psi i}(r_i)s_{\psi i}(t) \qquad s_{ui,\psi i}(t) = \dot{q}_{ui,\psi i}(t) \tag{4}$$

The vector of total absolute velocity on a node is the sum of rigid-body velocities at O_f and the generalized structural velocities at that node. From Eqs. (3) and (4), the velocity vector on a node of the fuselage is expressed as [2]:

$$\overline{V}_f(r_f,t) = C_f V_f + (\tilde{r}_f + \tilde{z}_f)^T C_f \Omega_f + \tilde{r}_f^T \dot{\psi}_f + \dot{z}_f$$
$$= C_f V_f + \tilde{r}_f^T C_f \Omega_f + (\widetilde{C_f\Omega_f})(\phi_{uf}q_{uf} + \tilde{y}_f\phi_{\psi f}q_{\psi f})$$
$$+ (\tilde{r}_f^T + \tilde{y}_f)\phi_{\psi f}s_{\psi f} + \phi_{uf}s_{uf} \tag{5}$$

The deflection of the attachment point of wings or empennage on the fuselage is a function of rotation angles due to deflections in bending and torsion of the fuselage. Figure 3 shows the kinematics of the attachment point O_w of the two halves of the wing on the aft fuselage, where the beams representing the aft fuselage and the left wing is depicted in the form of lumped mass m_f and m_w, respectively, with their respective stiffness elements. The other components are not shown for the sake of brevity. The point O_w is deflected by z_{fy} and z_{fz} in y and z directions, respectively, with a torsion angle of ψ_{fx} along the x axis. By using the first of Eq. (3), the rotation angle along the y axis due to bending in z axis is as follows:

$$\alpha_{fy}(r_{fi},t) = -\frac{\partial z_{fz}}{\partial r_{fi}} = -\left(\frac{\partial \phi_{uf}(r_{fi})q_{u_zf}(t)}{\partial x_f} + y_{fz}\frac{\partial \phi_{\psi f}(r_{fi})q_{\psi f}(t)}{\partial x_f}\right) \tag{6}$$

Similarly, the rotation angle along the z axis due to bending in the y axis is as follows:

$$\alpha_{fz}(r_{fi},t) = \frac{\partial z_{fy}}{\partial r_{fi}} = \left(\frac{\partial \phi_{uf}(r_{fi})q_{u_yf}(t)}{\partial x_f} + y_{fy}\frac{\partial \phi_{\psi f}(r_{fi})q_{\psi f}(t)}{\partial x_f}\right) \tag{7}$$

The generalized rotational velocities due to bending can be written in a vector form as:

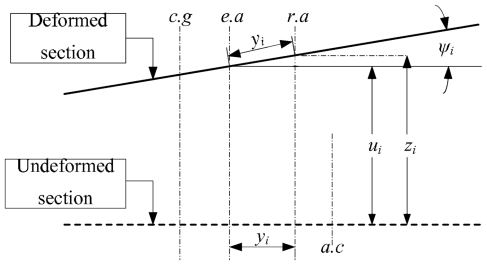

Fig. 2 Deformed section.

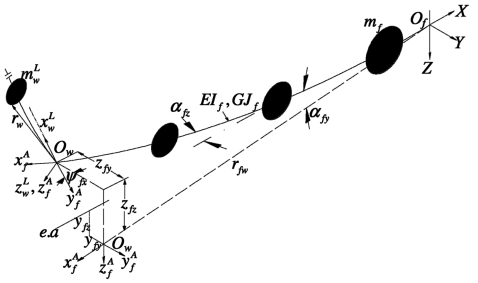

Fig. 3 Deflected aft fuselage beam.

$$\dot{\alpha}(r_{fi},t) = \Delta\phi_{ufi}s_{uf} + \tilde{y}_f\Delta\phi_{\psi fi}s_{\psi f}$$

$$\Delta = \begin{bmatrix} \partial/\partial x_f & 0 & 0 \\ 0 & 0 & -\partial/\partial x_f \\ 0 & \partial/\partial x_f & 0 \end{bmatrix}$$

$$\phi_{ufi}(r_{fi}) = \begin{bmatrix} 0 & 0 & 0 \\ 0 & \phi_{ufy} & 0 \\ 0 & 0 & \phi_{ufz} \end{bmatrix}$$

$$\phi_{\psi fi}(r_{fi}) = [\phi_{\psi f} \quad 0 \quad 0]^T$$

$$s_{uf} = [0 \quad \dot{q}_{u_y f} \quad \dot{q}_{u_z f}]^T$$

$$y_f = [0 \quad y_{fz} \quad y_{fy}]^T \tag{8}$$

The vector of total absolute velocity on a node of either the wing or the empennage is the sum of rigid-body and structural velocities of the aft fuselage, structural velocities of the attachment point O_i, and finally the structural velocities of the node itself. By using Eqs. (3), (4), and (8), the velocity vector on a node of a component i is expressed as

$$\begin{aligned} V_i(r_i,t) = {} & C_iV_f + C_i\tilde{r}_{fi}^T\Omega_f + C_i(\widetilde{\phi_{ufi}q_{uf}} + \tilde{y}_f\widetilde{\phi_{\psi fi}q_{\psi f}})^T\Omega_f \\ & + \tilde{r}_i^TC_i\Omega_f + (\widetilde{\phi_{ui}q_{ui}} + \tilde{y}_i\widetilde{\phi_{\psi i}q_{\psi i}})^TC_i\Omega_f \\ & + \tilde{r}_i^TC_i(\Delta\phi_{ufi}s_{uf} + (\tilde{y}_f\Delta\phi_{\psi fi} + \phi_{\psi fi})s_{\psi f}) \\ & + C_i(\phi_{ufi}s_{uf} + (\tilde{y}_f + \tilde{r}_{fi}^T)\phi_{\psi fi}s_{\psi f}) + (\tilde{y}_i + \tilde{r}_i^T)s_{\psi i} \\ & + \phi_{ui}s_{ui} \qquad i = w, e \end{aligned} \tag{9}$$

The velocity terms in Eqs. (5) and (9) are sorted out in a vector form as shown in Eq. (2) and then used in Eq. (1). The coefficients resulting from the product of velocities construct the global mass matrix $M = [M_{jk}]$. Readers are referred to [2] for the complete listing of the submatrices $[M_{jk}]_i$ of the mass matrix except for the modified submatrices due to bending–torsion coupling. These are given in Eqs. B3–B8 of the previous version of this paper [16].

The potential energy is presented in the form of strain energy [12,17]:

$$U = \sum_{i=f,e,w}\int\frac{1}{2}[EI_i(z_i'')^2 - 2k_i(z_i'')(\psi_i') + GJ_i(\psi_i')^2]dD_i \tag{10}$$

The global stiffness matrix of the aircraft is a function of the strain energy [18]:

$$K = [K_{jk}] = \left[\frac{\partial^2U}{\partial q_j\partial q_k}\right] \tag{11}$$

Using Eqs. (3), (10), and (11), the cross coupling term in the form of a submatrix of the global stiffness matrix is as follows:

$$\begin{aligned} K_{u\psi i} &= \left[\frac{\partial^2U}{\partial q_u\partial q_\psi}\right] \\ &= \overbrace{[\phi_{ui}'']\mathrm{diag}[EI_{i(\mathrm{dof})1}\cdots EI_{i(\mathrm{dof})n}]\mathrm{diag}[y_{i1}\cdots y_{in}][\phi_{ui}'']^T}^{\text{due to the use of } r.a} \\ &\quad - \underbrace{[\phi_{ui}'']\mathrm{diag}[k_{i1}\cdots k_{in}][\phi_{ui}']^T}_{\text{due to the material anisotropy}} \end{aligned} \tag{12}$$

where

$$[\phi_i] = \begin{bmatrix} \phi_{1,1} & \cdots & \phi_{1,n} \\ \phi_{2,1} & \cdots & \phi_{2,n} \end{bmatrix}, \qquad i = u, \psi$$

The generalized momenta p can be expressed as a partial derivative of Lagrangian "$L = T - U$" to the velocity [2,18]:

$$p = \partial L/\partial V = MV \qquad p = [\,p_{vf}^T \quad p_{\Omega f}^T \quad p_{uf}^T \quad \cdots \quad p_{\psi e}^T\,] \tag{13}$$

By using the generic form of equations of motion [2], the equations of motion for the whole aircraft can be expressed as given in Eq. 22 of [2], where the expression of the generalized momenta for the elastic motion in torsion is modified due to the inclusion of bending–torsion coupled vibrations:

$$\dot{p}_{\psi i} = \frac{\partial T}{\partial q_{\psi i}} - K_{\psi i}q_{\psi i} - C_{\psi i}s_{\psi i} + \mathbf{Q}_{\psi i} \qquad i = w, e \tag{14}$$

The equations of motion solve a state vector of 76 elements, which include 38 generalized coordinates, 6 rigid-body translations and rotations, and 32 elastic deformations. The equations contain all lower and higher frequency modes. To determine the lower frequencies and corresponding aircraft shape functions (ASF), the modal is reduced to fewer degrees of freedom by the eigenvalue solution of global stiffness and mass matrices (i.e., $[K - \lambda M_{q=0}]d = 0$). See the process of reduction in Eqs. 11–20 of Ref. [19].

The theory of extended aeroelasticity [2,19,20] considers the elastic motions or vibrations about steady state to be smaller in magnitude to those of rigid-body motions. The equations of motion are linearized around a steady-state condition and distinguished into two forms (i.e., the zero-order problem and first-order problem). The zero-order problem, which represents the rigid-body motion can be written in state-space form as

$$\dot{x}^{(0)}(t) = A^{(0)}(t)x^{(0)}(t) + B_u^{(0)}(t)u^{(0)}(t) + \begin{bmatrix} e_1 \\ F_f \\ M_f \end{bmatrix} \tag{15}$$

Equation (15) introduces the zero-order state vector $x^{(0)} = [\,R_f^{(0)T} \quad \theta_f^{(0)T} \quad p_{vf}^{(0)T} \quad p_{\Omega f}^{(0)T}\,]^T$ that represents the rigid motions and momenta with respect to inertial axes and aircraft body axes, respectively. The coefficient matrix $A^{(0)}$ times the state vector $x^{(0)}(t)$ gives a zero-order force vector due to inertia. $B_u^{(0)}$ times $u^{(0)}(t)$ gives a zero-order force vector due to control inputs. The vectors F_f and M_f are resultant forces and moments, respectively, due to aerodynamics and gravity loads. The first-order problem, a linearized state around the steady-state, takes account of vibrations and their effects on the overall response of the aircraft:

$$\dot{x}^{(1)}(t) = [A^*(t) + B_x(t) - B_u(t)G]x^{(1)}(t) + \begin{bmatrix} e_2 \\ F_{\mathrm{ext}}(t) \end{bmatrix} \tag{16}$$

The first-order state vector contains two additional subvectors of generalized coordinates and their momenta:

$$x^{(1)} = [\,R_f^{(1)T} \quad \theta_f^{(1)T} \quad \xi^T \quad p_{vf}^{(1)T} \quad p_{\Omega f}^{(1)T} \quad p_\eta^T\,]^T \tag{17}$$

The state matrix A^* contains the partial derivatives of zero-order velocities, stiffness, and damping matrices with respect to the first-order state vector. The coefficient matrix B_x gives the sum of aerodynamic and gravitational forces and subsequent moments due

to vehicle motion resulting from external disturbance F_{ext}. B_u multiplied by the closed-loop gain matrix G gives the forces and moments due to first-order control inputs $u^{(1)}$, which consequently minimize the effects of external disturbance. The gain matrix G can be obtained by optimizing the performance index of a linear quadratic regulator [2,21]:

$$J(x^{(0)}, u^{(0)}) = \int_0^t (x^{(0)T} Q x^{(0)} + u^{(0)T} R u^{(0)}) \mathrm{d}t \tag{18}$$

where

$$u^{(1)}(t) = -G(t) x^{(1)}(t)$$

Full expressions for all the matrices like $A^{(0)}$, A^*, B_x, and B_u can be found in Eqs. 7, 28, and 49 of [20], except the modified version of submatrices of A^* are given in Eqs. C1–C4 of the previous version of this paper [16]. The vector of external disturbance due to gust is obtained through time domain solution of Eq. (15):

$$\begin{bmatrix} e_2 \\ F_{\text{ext}}(t) \end{bmatrix} = B_x(t) \begin{bmatrix} e_2 \\ M_\xi^{(0)} x_{R\theta}^{(0)}(t) \end{bmatrix} \tag{19}$$

in which $x_{R\theta}$ is $[\, R_f^{(0)T} \quad \theta_f^{(0)T} \quad e_m \,]^T$ and e_m is a null vector of size $(1 \times m)$. The final perturbed solution will be as follows [2]:

$$x(t) = x^{(0)}(t) + x^{(1)}(t) \qquad u(t) = u^{(0)}(t) + u^{(1)}(t) \tag{20}$$

III. Dynamic Loads Model

Dynamic loads can be predicted at each node by calculating the rate of change of momentum due to elastic motions of that node:

$$\dot{p}_\eta = \frac{d}{dt} \begin{bmatrix} p_{ui} \\ p_{\psi i} \end{bmatrix} = \begin{bmatrix} F_{di} \\ M_{di} \end{bmatrix} \tag{21}$$

Solving the equations of motion in the form of momenta gives an extra advantage for solving the dynamic loads [7,22]. The numerical solution of Eq. (16) gives the first-order momenta, which are then used to calculate first-order velocities. The first-order velocities can be expressed by linearizing Eq. (13) as [20]

$$V_\eta^{(1)}(t) = (M_\xi^{(0)})^{-1} (p^{(1)}(t) - M_\xi^{(1)} V_\eta^{(0)}) \tag{22}$$

The reduced first-order velocity vector $V_\eta^{(1)}$ is expressed as $[\, V_f^{(1)T} \quad \omega_f^{(1)T} \quad \eta^T \,]^T$. After the numerical solution, Eq. (16) eventually acts as an algebraic equation, which gives the momenta rates $\dot{p}$. It is known that the mass matrix is a function of generalized coordinates q [22], and does not depend upon the generalized velocities s, that is, for a linear time invariant system the time derivative of mass matrix around the steady-state is zero, which states the time derivative of Eq. (22) as:

$$\dot{V}_\eta^{(1)}(t) = (M_\xi^{(0)})^{-1} \dot{p}^{(1)}(t) \tag{23}$$

The reduced-order dynamic loads vector L_η can be expressed by the summation of forces method (SFM), and that is defined as the summation of all the aerodynamic and inertial loads [14]:

$$\begin{bmatrix} e_2 \\ L_f(t) \\ L_\eta(t) \end{bmatrix} = \overbrace{(B_x - B_u G) x^{(1)}(t) + \begin{bmatrix} e_2 \\ F_{\text{ext}}(t) \end{bmatrix}}^{\text{aerodynamic loads}} - \underbrace{\begin{bmatrix} e_2 \\ (M_\xi^{(0)}) \dot{V}_\eta^{(1)}(t) \end{bmatrix}}_{\text{inertial loads}} \tag{24}$$

which is then expanded to a full-order vector for a particular component by using the matrices of eigenvector and shape functions:

$$\begin{aligned} F_{di}^{\text{SFM}}(r_i, t) &= [\phi_{ui}(r_i) D_{ui} + y_i \phi_{\psi i}(r_i) D_{\psi i}] L_\eta^{(1)}(t) \\ M_{di}^{\text{SFM}}(r_i, t) &= \phi_{\psi i}(r_i) D_{\psi i} L_\eta^{(1)}(t), \qquad i = f, w, e \end{aligned} \tag{25}$$

where F_{di} and M_{di} are the vectors of vertical shear force and torsional moment along the $r.a$, respectively. Upward shear is negative and a bending moment that produces tension in the upper fiber is considered positive. The torsional moment on a node follows the sign convention of a particular component, see Fig. 1. Loads calculated from SFM can be verified by using the mode displacement method (MDM), which is based on the internal forces, caused by the structural deformations due to aerodynamic and inertial loads [14,23]:

$$\begin{aligned} F_{di}^{\text{MDM}}(r_i, t) &= [\phi_{ui}(r_i) D_{ui} + y_i \phi_{\psi i}(r_i) D_{\psi i}] K_\xi \xi^{(1)}(t) \\ M_{di}^{\text{MDM}}(r_i, t) &= \phi_{\psi i}(r_i) D_{\psi i} K_\xi \xi^{(1)}(t), \qquad i = f, w, e \end{aligned} \tag{26}$$

IV. Numerical Example

A twin-jet aircraft is selected as a test case for response and dynamic loads over a discrete gust. The aircraft structural and aerodynamic data are given in [2]. Flight conditions for symmetric flight are presented in Table 1. All previous equations are combined in one Matlab program known as DARLoads [7,22]. It simulates the response and dynamic loads of a fully flexible aircraft. After reading the inputs of structural and aerodynamic models, the full-order matrices of mass, stiffness, and damping are constructed. With respect to the aircraft body axes, a fixed point is selected on each component of the aircraft as a practical $r.a$ of the component vibrations. To study the effects of the bending–torsion coupling on the natural properties and response of the aircraft, it is assumed that during a structural optimization exercise the $e.a$ of each wing and horizontal tail exhibits a straight line and changes its position. For this purpose three different cases of $e.a$ positions are simulated. In the first case the $e.a$ of each wing and horizontal tail is placed 30.0 mm in front of their particular $r.a$, in the second case these are aligned, and in the third case the $e.a$ of each wing and horizontal tail is placed 30.0 mm behind their particular $r.a$, see Table 2. It is to be noted that the forward or rearward directions are to be referred to with respect to aircraft body axes O_f, however, the sign convention of a particular y_i is taken with respect to its local axes system O_i, see Fig. 1.

A. Static Analysis

The steady state under a purely longitudinal flight condition, as given in Table 1, is achieved by using an iterative optimization algorithm, which balances out the forces and moments around the body axes of the aircraft by minimizing a quadratic cost function of the zero-order state vector of Eq. (15) [22]. The optimal values for elevator, aileron, and rudder deflection with throttle setting, respectively, in case 1 are found to be $u^{(0)} = [1.55\,\text{deg}, 0, 0, 76.4\%]$. Similarly the optimal zero-order pitch-angle $\theta_{f\Theta}^{(0)}$ is found to be 0.55

Table 1 Geometry and flight conditions

Airspeed $V^{(0)}$, m − s^{-1}	250.0
Altitude, m	7620.0
Wing span, m	16.7
Wing root chord, m	3.287
Horizontal tail root chord, m	1.6263
Mass, Kg	5884.23
Inertia $I_{xx}^{(0)}$, Kg − m^2	20708.91
Inertia $I_{yy}^{(0)}$, Kg − m^2	64003.38
Inertia $I_{zz}^{(0)}$, Kg − m^2	79590.5
Inertia $I_{xy}^{(0)}$, Kg − m^2	0.8072
Inertia $I_{xz}^{(0)}$, Kg − m^2	−4241.35

Table 2 Three cases of $e.a$ position

Case Number	y_w^R, y_e^R	y_w^L, y_e^L
1	−30.0 mm	30.0 mm
2	0.0 mm	0.0 mm
3	30.0 mm	−30.0 mm

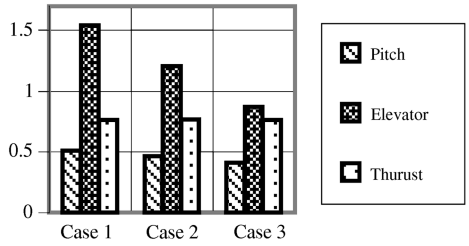

Fig. 4 Optimal trim variables.

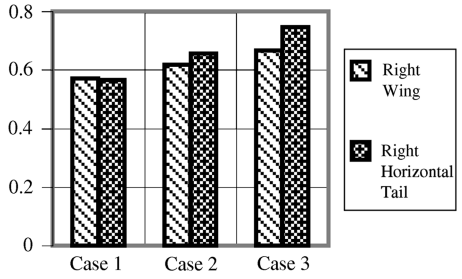

Fig. 5 Static twist angles, deg.

deg. The static upward bending deflection of 1.236 m and 0.168 m is calculated at the tip of each wing and horizontal tail, respectively. Figure 4 shows the change in trim solutions of pitch and elevator deflection for three cases of the elastic axis position. The change in the values of pitch-angle and elevator deflection is less than 0.1 and 0.66 deg, respectively, and the throttle setting is changing not more than 1.0%. It also shows that the elevator deflection decreases while the *e.a* moves from front to the rear of *r.a*. The static torsion deflections of both wings and horizontal tails also change with the position of their particular elastic axes. Figure 5 shows that the local twist angles at the tip of both the wing and horizontal tail increases as the *e.a* moves from front to the rear of *r.a*. Figure 6 explains this phenomenon where the locations of the key points on the tip sections of both the right wing and horizontal tail are shown. It shows the actual locations of the aerodynamic centers (*a.c*), centers of mass (*c.g*), *r.a*, and the rearward position of *e.a* (i.e., case 3 in Table 2). The abscissa of Fig. 6 gives the section lengths in meters. In the case of the wing tip, the *c.g* of the tip section is located quite close to the *r.a* and whenever during the analysis the *e.a* coincides or positioned in the front of *r.a*, the torque around the *e.a* produced by weight is added to the torque produced by the aerodynamic loads. However, both of these torques oppose each other when the *e.a* is positioned rearward of the *r.a*. The vertical aerodynamic force on the wing tip, at the given speed, is approximately seven times larger than its weight, which, on the other hand, due to increase in moment arm makes the twist angle a bit larger than to those of the cases where the *e.a* is placed ahead of the *c.g*. Similarly in the case of the horizontal tail tip section the aerodynamic force, at the given speed, is approximately three times larger than its weight. The torque produced by the aerodynamic force, for all the positions of *e.a*, is deducted by the torque produced by the weight, where the moment arm of the aerodynamic force makes the horizontal tail to twist more when the *e.a* is positioned rearward of the *r.a*. It is also noted that as the twist angle increases at the horizontal tail, the elevator deflection decreases and vice versa. As we know, apart from the rigid-body pitch angle and the throttle input, the lift required in trimming the aircraft is also contributed by both twist over the tailplane and the elevator deflection. So it would be correct to state that the optimization routine used here efficiently optimizes the elevator deflection against the given structural deformations.

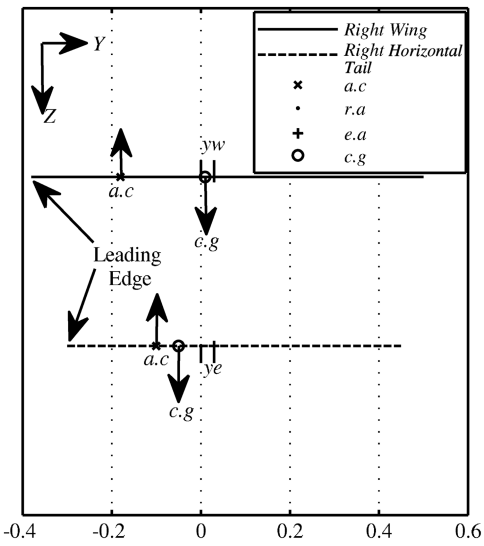

Fig. 6 Tip sections, meters.

B. Model Reduction

As stated earlier, ASF are determined by eigenvalue solution of global mass and stiffness matrices. Table 3 describes the shapes for the first 20 ASF in which, for example, "W-B" means that wing bending is the predominant feature of the particular ASF and similarly "H-T" indicates the predominance of torsion in the horizontal tail. To have the greatest impact of aerodynamics force and moments, it is thought to consider a sufficient number of ASF of lower to higher frequencies, while exhibiting both bending and torsion as predominant features in wings and horizontal tails. By using the first 18 ASF that cover the frequencies until 53.7 Hz, the full-order model in each simulation case is reduced to only 24 DOF, that is, 6 rigid-body and 18 elastic degrees of freedom. Figure 7 shows the first six ASF. The higher frequency ASF are not shown here for the sake of brevity.

C. Dynamic Analysis

The aircraft is subjected to a 1-cosine vertical gust $w_g(t)$ of 5.0 m-sec^{-1} over a period of 4.0 s. The resultant forces and moments in vector $[e_1^T \quad F_f^T \quad M_f^T]^T$ of Eq. (15) are a function of pitch angle $\theta_{i\Theta}^{(0)}$. The input for the rigid-body response simulation is given as the

Table 3 Description of first 12 ASF

ASF Number	Frequency, Hz	Predominate Shape[a]	ASF Number	Frequency, Hz	Predominate Shape[a]
1	5.92	First symmetric W-B	11	26.58	Second symmetric F-B
2	8.26	First asymmetric W-B	12	27.42	Second asymmetric W-B
3	10.45	First symmetric H-B	13	37.72	First asymmetric F-T
4	11.24	First asymmetric H-B	14	46.81	First asymmetric H-T
5	12.32	Second asymmetric H-B	15	49.91	Second asymmetric H-T
6	14.64	Second symmetric H-B	16	53.02	First symmetric H-T
7	19.51	First asymmetric V-B	17	53.37	First asymmetric W-T
8	20.09	First asymmetric F-B	18	53.70	Second symmetric H-T
9	22.05	Second asymmetric V-B	19	62.42	Third asymmetric H-T
10	23.05	First symmetric F-B	20	64.60	Third symmetric H-T

[a]B: Bending, F: Fuselage, H: Horizontal tail, T: Torsion, W: Wings, V: Vertical tail

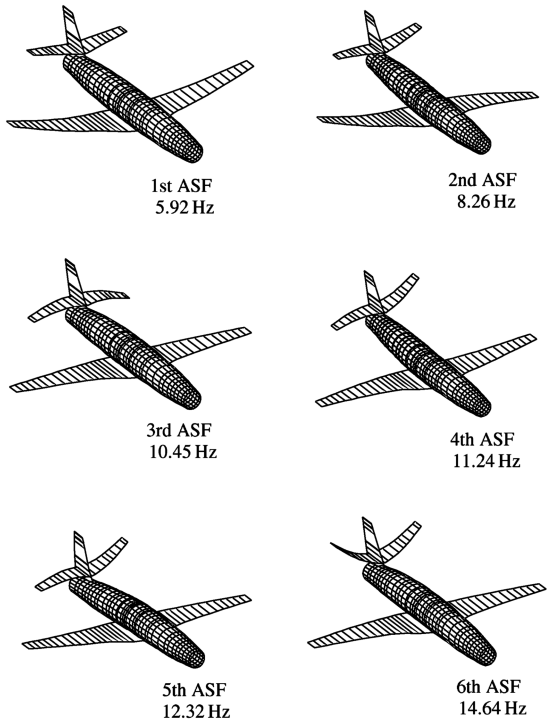

Fig. 7 First six ASF.

disturbance in the rigid-body pitch angle. To simulate the pitch rate effects, the plunge velocities $\dot{R}_{iz}$ at the wing and horizontal tail are different with a factor of distance l_i between their aerodynamic centers to O_f (i.e., $\dot{R}^{(0)}_{iz} = \dot{R}^{(0)}_{fz} + l_i\dot{\theta}^{(0)}_{f\Theta}$). Where $\theta^{(0)}_{i\Theta}$ is given as $\frac{w_g(t)+\dot{R}^{(0)}_{iz}}{V_{fx}} + \theta^{(0)}_{f\Theta}$ [24]. The solution of Eq. (15) in the form of plunge and pitching velocities is shown in Figs. 8 and 9, respectively.

The solution of Eq. (15) is used in Eq. (19) to obtain the vector F_{ext}. Equation (16) is solved to acquire the first-order aircraft dynamic response. The weighting matrices in Eq. (18) are taken as $Q = 250I$ and $R = \text{diag}[10^5, 10^5, 10^5, 10^6]$, where I is the identity matrix of size (6×6). Despite the purely symmetric inputs, the presence of the product of inertia I_{xy}, given in Table 2, rolls the aircraft. The first-order pitching $\theta^{(1)}_{f\Theta}$ and rolling $\theta^{(1)}_{f\Phi}$ response of the aircraft with the control inputs are plotted in Fig. 10. The disturbances with

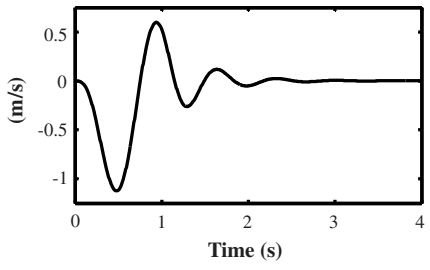

Fig. 8 Rigid-body plunge velocity.

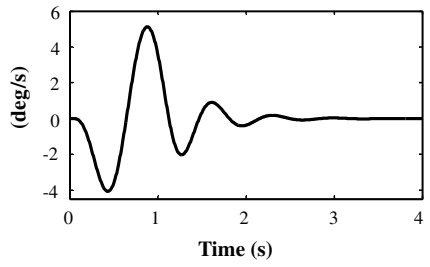

Fig. 9 Rigid-body pitching velocity.

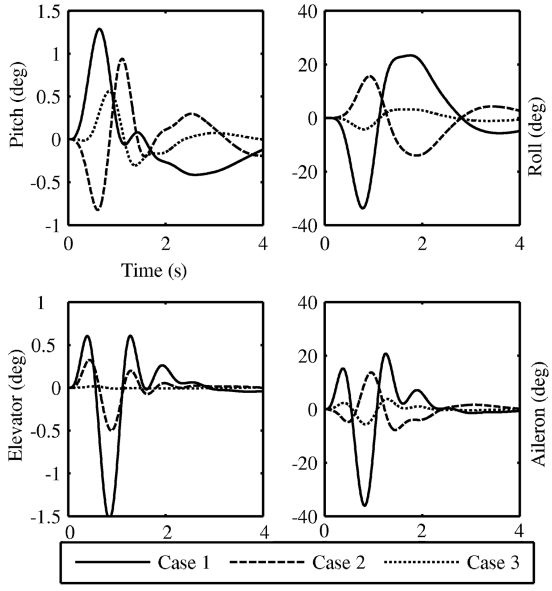

Fig. 10 First-order response and control.

subsequent control input are quite high for the first two cases, given in Table 2. However, there is a sudden decrement in the magnitudes for the third case.

To obtain the structural loads, the time domain solution of Eq. (16) is then used in Eqs. (22–26). The comparison of shear forces from SFM and MDM load equations is presented in Fig. 11. It shows that in the case of wings and horizontal tails the results are in fair agreement, but in the case of the aft fuselage the magnitude of shear force calculated from MDM is lesser than to that of FSM. The reason can be the total numbers of ASF with the predominant fuselage deformations in model reduction. The numbers of ASF to be used in model reduction can be identified through the frequency plots, where it gives a fair idea of each ASF or mode shape affecting the response [23].

Figures 12–14 show the deflections and corresponding loads at tips and roots of right wing, fuselage, and right horizontal tail, respectively. The wing is deflecting vertically around its equilibrium position from 0.2 m upward to 0.18 m downward over different positions of $e.a$, and meanwhile twisting up at 0.086 deg to twisting

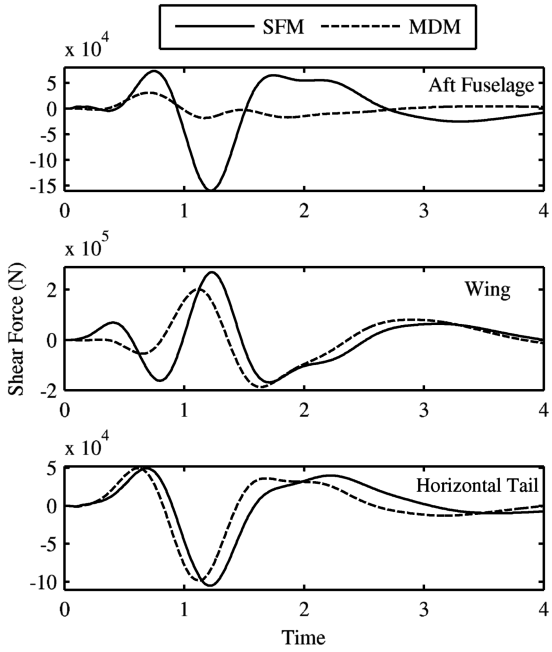

Fig. 11 Shear forces at the root.

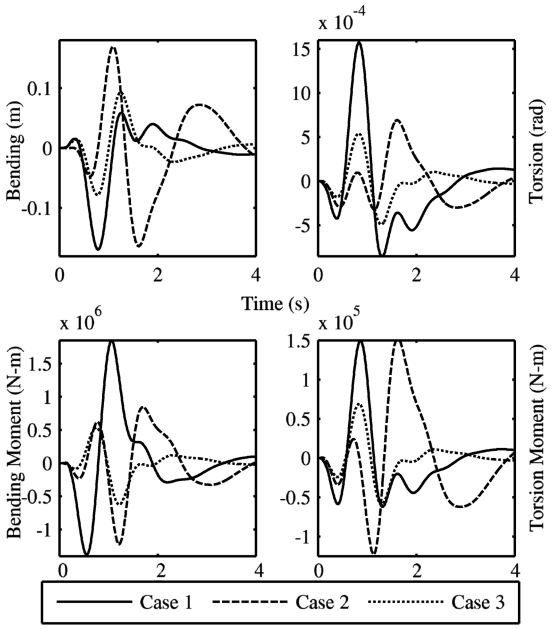

Fig. 12 Wing tip deflections and root loads.

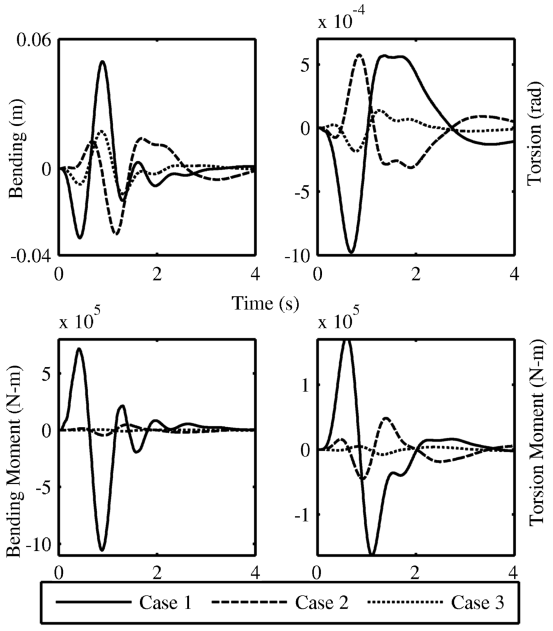

Fig. 13 Aft fuselage tip deflections and root loads.

down at 0.028 deg. Similarly, the root of horizontal tail, that is the aft fuselage tail is bending upward from 0.035 to 0.055 m downward, while the tip of horizontal tail is twisting with torsional angles of −0.23 to 0.515 deg.

Similar to the $\theta^{(1)}_{f\Theta}$ and $\theta^{(1)}_{f\Phi}$, the amplitude of structural deformations of a component are also reduced significantly when the $e.a$ is positioned to the rearward of the $r.a$. This looks contrary to the situation stated in the case of static analysis where the twist angle on tip sections increases when the $e.a$ moves from front to the rear. The main reason is the role of inertial terms during dynamic response analysis whereas in finding the static deformations these terms do not play an active role. The situation shown in Fig. 6 is not the same for every section of the wings and the empennage, because the position of $c.g$ of every section varies with respect to their respective $r.a$. Moreover, the value of y_i should also be different for every section on both wings and empennage. However, as stated earlier, it is assumed to be constant all over the length of a component, which at least gives

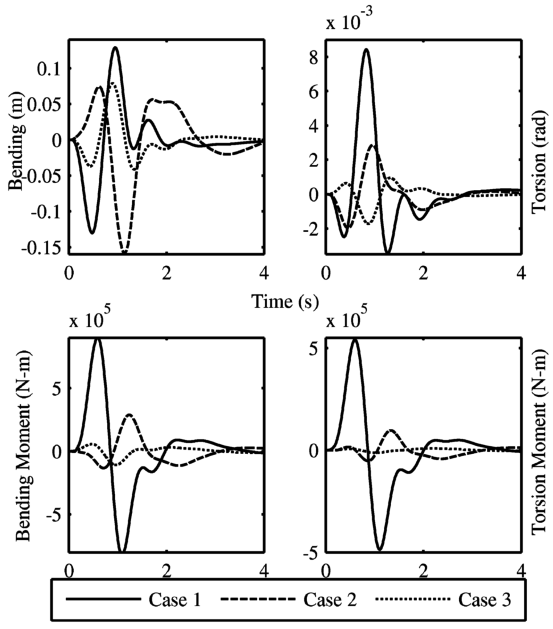

Fig. 14 Horizontal tail tip deflections and root loads.

a quite good picture of the effects of bending–torsion coupling on the aircraft dynamic response and also shows the relevance of proper mathematical modeling.

V. Conclusions

The modified equations of motion with coupled vibrations in the aircraft components were found to be very useful. The position of elastic axis, with respect to a fixed $r.a$ in each wing and tail structure, plays a significant role in the dynamics of the fully flexible aircraft. These effects were not clearly known because the $e.a$ was either used as the reference of vibrations or the modeling and simulation of the $e.a$ position was restricted to a wing in flutter analysis. Although for a structural design engineer the cases of $e.a$ positions, given herein, do not seem to be a proper way of doing an analysis, it does give a fair picture in conceptual or preliminary design. However, the modified equations remove the necessity of using an elastic axis as a reference of vibration.

Optimization of aircraft structural components with new stiffness and mass matrices in each iteration and consequently the new sets of dynamic loads and stresses can be done more accurately with the modified equations. The mathematical model presented herein is equally capable of handling this kind of problem, for example, while using the gradient-based optimization routines, if one of the objectives is to minimize the vibrations and consequent loads then the loads equations based on stiffness can easily be differentiable to a structural design variable that yields the loads sensitivity of the each relevant design variable.

While looking at the scope of the mathematical modeling of flexible aircraft, the development presented in this paper does not end here. The generic equations of motion can be used for any type of aircraft, but the formulation of its subparts like mass and stiffness matrices vary with the configuration. The model presented in this paper is capable of simulating the dynamics of any conventional aircraft, which are believed to remain in service for at least next two decades. Looking at the proposed alternatives like blended wing-body or the Prandtlplane, a robust framework will be required in the future to automate the process of constructing the structural dynamics part of the inertially coupled equations of motion.

Acknowledgment

The first author acknowledges his colleague Mark Voskuijl for his assistance in writing.

References

[1] Patil, M. J., Hodges, D. H., and Cesnik, C. E. S., "Nonlinear Aeroelasticity and Flight Dynamics of High-Altitude Long-Endurance Aircraft," *Journal of Aircraft*, Vol. 38, No. 1, Jan.–Feb. 2001, pp. 88–94.
doi:10.2514/2.2738

[2] Tuzcu, I., and Meirovitch, L., "Integrated Approach to the Dynamics and Control of Maneuvering Flexible Aircraft," NASA CR-211748, 2003.

[3] Hofstee, J., Kier, T., Cerulli, C., and Looye, G., "A Variable Fully Flexible Dynamic Response Tool for Special Investigations (VARLOADS)," *Proceedings of the International Forum on Aeroelasticity and. Structural Dynamics*, AIAA, Reston, VA, June 2003.

[4] Milne, R. D., "Dynamics of the Deformable Aeroplane," British Aeronautical Research Council R&M 3345, Her Majesty's Stationery Office, England, 1964.

[5] Waszak, M. R., and Schmidt, D. K., "Flight Dynamics of Aeroelastic Vehicles," *Journal of Aircraft*, Vol. 25, No. 6, June 1988, pp. 563–571.
doi:10.2514/3.45623

[6] Weisstein, E. W., *CRC Concise Encyclopedia of Mathematics*, 2nd ed., Kluwer Academic, Norwell, MA, Dec. 2002.

[7] Baluch, H. A., Slingerland, R., and van Tooren, M. J. L., "Dynamic Loads Optimization During Atmospheric Turbulence on a Flexible Aircraft," *Proceedings of Young Persons Aerodynamic Conference*, Royal Aeronautical Society, Bristol UK, Oct. 2006.

[8] Guo, S., Cheng, W., and Cui, D., "Aeroelastic Tailoring of Composite Wing Structures by Laminate Layup Optimization," *AIAA Journal*, Vol. 44, No. 12, Dec. 2006, pp. 3146–3149.
doi:10.2514/1.20166

[9] Hong, C., and Chopra, I., "Aeroelastic Stability Analysis of a Composite Rotor Blade," *Journal of the American Helicopter Society*, Vol. 30, No. 2, 1985, pp. 57–67.

[10] Chandra, R., Stemple, A. D., and Chopra, I., "Thin-Walled Composite Beams Under Bending, Torsional, and Extensional Loads," *Journal of Aircraft*, Vol. 27, No. 7, 1990, pp. 619–626.
doi:10.2514/3.25331

[11] Smith, E., and Chopra, I., "Formulation and Evaluation of an Analytical Model for Composite Box-Beams," *Journal of the American Helicopter Society*, Vol. 36, No. 3, July 1991, pp. 23–35.

[12] Lottati, I., "Flutter and Divergence Aeroelastic Characteristics for Composite Forward Swept Cantilevered Wing," *Journal of Aircraft*, Vol. 22, No. 11, 1985, pp. 1001–1007.
doi:10.2514/3.45238

[13] Hodges, D. H., *Nonlinear Composite Beam Theory*, edited by F. K. Lu, Progress in Astronautics and Aeronautics, AIAA, Reston, VA, Vol. 213, 2006, pp. 71–88, Chap. 4.

[14] Bisplinghoff, L. R., Ashley, H., and Halfman, R. L., *Aeroelasticity*, Dover, New York, 1996, pp. 62–69, 440, 641–684, Chap. 10.

[15] Waszak, M. R., Buttrill, C. S., and Schmidt, D. K., "Modeling and Model Simplification of Aeroelastic Vehicles: An Overview," NASA TM-107691, 1992.

[16] Baluch, H. A., and van Tooren, M., "Modified Inertially Coupled Equations of Motion for a Flexible Aircraft with Bending-Torsion Coupled Beams," *Proceedings of the International Forum on Aeroelasticity and. Structural Dynamics*, AIAA, Reston, VA, June 2007.

[17] Hodges, D. H., "Bending-Torsion Divergence of a Clamped-Clamped Composite Wing," *Journal of Aircraft*, Vol. 44, No. 6, Nov.–Dec. 2007, pp. 2070–2072.
doi:10.2514/1.28686

[18] Meirovitch, L., *Principles and Techniques of Vibrations*, Prentice–Hall, Upper Saddle River, New Jersey, 2000, Chap. 4.4.

[19] Meirovitch, L., and Tuzcu, I., "Time Simulations of the Response of Maneuvering Flexible Aircraft," *Journal of Guidance, Control and Dynamics*, Vol. 27, No. 5, Sept.–Oct. 2004, pp. 814–828.
doi:10.2514/1.2392

[20] Meirovitch, L., and Tuzcu, I., "Control of Flexible Aircraft Executing Time-Dependent Maneuvers," *Journal of Guidance, Control and Dynamics*, Vol. 28, No. 6, Nov–Dec. 2005, pp. 1291–1300.
doi:10.2514/1.12774

[21] Sobieszczanski–Sobieski, J., Bloebaum, C. L., and Hajela, P., "Sensitivity of Control-Augmented Structure Obtained by a System Decomposition Method," *AIAA Journal*, Vol. 29, No. 2, 1991, pp. 264–270.
doi:10.2514/3.10573

[22] Baluch, H. A., Lisandrin, P., Slingerland, R., and van Tooren, M., "Effects of Flexibility on Aircraft Dynamic Loads and Structural Optimization," *45th AIAA Aerospace Sciences Meeting and Exhibit*, AIAA Paper 2007-768, Jan. 2007.

[23] Pototzky, A. S., and Perry, B., "New and Existing Techniques for Dynamic Loads Analysis of Flexible Airplanes," *Journal of Aircraft*, Vol. 23, No. 4, April 1986, pp. 340–347.
doi:10.2514/3.45309

[24] Wright, J. R., Cooper, J. E., *Introduction to Aircraft Aeroelasticity and Loads*, AIAA Education Series, AIAA, New York, 2007, pp. 303–305, Chap. 16.